Comparison of SALVUS and QSEIS Synthetic Seismograms in Homogeneous and Layered Half-Space

Soumen Koley, Hadrien Michel
University of Liege

1 Introduction

In this note we compare synthetic seismograms generated using two widely used numerical solvers for elastic wave propagation: `SALVUS` and `QSEIS`. Our aim is to assess whether both codes produce consistent wavefields in a controlled, idealized configuration, and to identify and explain any systematic differences that arise from differences in source representation rather than physics.

We focus first on the simplest configuration: a homogeneous elastic half-space with constant V_P, V_S, and density. In this setting, the Green's functions are known analytically, there is no velocity contrast, no scattering, and therefore no dispersion of body or surface waves. Any differences observed between synthetic seismograms must therefore originate from the source-time function, numerical implementation, or convention rather than from propagation physics.

2 Solvers and Source-Time Functions

Both codes solve the 3-D elastic wave equation but employ different numerical strategies.

- `SALVUS` solves the full wave equation in the time domain using high-order finite elements. The user supplies an arbitrary source-time function. For this study, a broadband pulse with nearly flat amplitude in 2 Hz to 10 Hz was used.
- `QSEIS` solves the wave equation using a frequency-domain reflectivity method. When no source-time function is supplied, `QSEIS` uses a default "delta-like" pulse given by

$$w(t) = \frac{2}{\tau}\,\sin^2\!\left(\frac{\pi t}{\tau}\right), \qquad 0 < t < \tau, \tag{1}$$

  where τ is the pulse duration. In practice, τ is specified in samples and converted to seconds by $\tau = n_{\text{sam}}\,\Delta t$.

For the default choice $n_{\text{sam}} = 4$ and $\Delta t = 0.02\,\text{s}$, the pulse duration is $\tau = 0.08\,\text{s}$, and its center of energy is approximately $\tau/2 = 0.04\,\text{s}$. Thus the `QSEIS` default wavelet is broadband but exhibits a *causal time shift* of two samples.

By contrast, the `SALVUS` wavelet used here is approximately zero-phase and centered at $t = 0$. Figures 1(a) and (b) show the `SALVUS` and the `QSEIS` wavelets in time domain. Unlike the `SALVUS` wavelet which is zero phase wavelet, implying it has maximum energy at zero time and symmetric spread in both causal and acausal branches, the QSEIS wavelet is a minimum phase wavelet with a finite causal support. The absolute value of the magnitud of the Fourier transforms are shown in Figures 1(c) and (d) corresponding to the `SALVUS` and the `QSEIS` wavelets, respectively. The SALVUS wavelet is band-limited with its dominant energy in the 2 – 8 Hz band. On the contrary the `QSEIS` wavelet have energy spread in the entire Nyquist band.

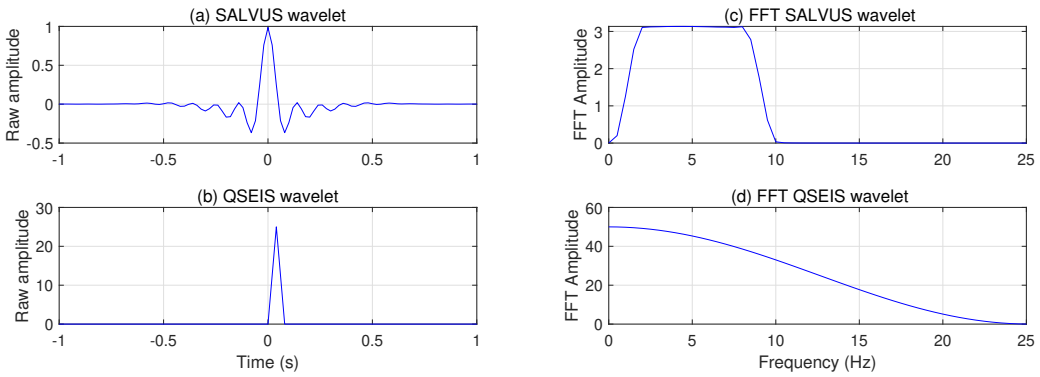

Figure 1: (a) Time domain representation of the `SALVUS` zero phase wavelet with symmetric spread across $t = 0$. (b) `QSEIS` wavelet in time domain representing a physical delta function like triangular pulse lasting for just four time samples. (c) Absolute amplitude of the FFT of the `SALVUS` wavelet shwing its bandlimited nature in teh frequency band $2 - 8$ Hz. (d) Absolute amplitude of the FFT of the `QSEIS` wavelet showing a much broader spectral content. All wavelets are resampled to 50 Hz for consistent representation.

3 Interpretation of `QSEIS` and `SALVUS` Green's Functions

In this section we clarify what the Green's functions produced by `QSEIS` and `SALVUS` represent, how the source radiation patterns differ between the two solvers, and how to construct a consistent set of displacement Green's functions for subsequent ambient noise simulations or waveform synthesis.

3.1 Green's functions produced by `QSEIS`

`QSEIS` works in the frequency–wavenumber domain for a 1-D layered medium. For each requested source type, it computes the displacement response at the receivers for unit forces acting in a fixed coordinate system where:

- the *downward vertical* direction corresponds to the positive z axis,
- the *radial* direction corresponds to the horizontal direction pointing from the source toward the receiver (North), and
- the *transverse* direction is perpendicular to the radial direction (East).

When the user requests Green's functions for a vertical force (`fz-*` files), `QSEIS` returns only the vertical (z) and radial (r) components. This is physically expected: a purely vertical point force in an azimuthally symmetric 1-D medium cannot produce any transverse displacement. The system has no preferred horizontal direction, and the SH motion is decoupled from the P–SV system.

In contrast, when the user requests Green's functions for a horizontal force (`fh-*` files), `QSEIS` internally decomposes that horizontal force into two orthogonal components:

1. a component *along* the source–receiver line (radial), and
2. a component *perpendicular* to that line (transverse).

Thus a single "horizontal" directive in the input file produces *both* P–SV (radial + vertical) and SH (transverse) Green's functions. The user therefore obtains:

$$G_z^{(h)}(t), \quad G_r^{(h)}(t), \quad G_t^{(h)}(t),$$

where the superscript (h) denotes a unit horizontal force, which `QSEIS` resolves relative to the source–receiver geometry. This interpretation is crucial: the transverse response in `QSEIS` *does not* imply that the force had a transverse component in the user's coordinate system—it is introduced automatically.

3.2 Green's functions produced by `SALVUS`

`SALVUS`, being a full 3-D solver, does not make the implicit symmetry assumptions of `QSEIS`. A force direction must be specified explicitly in the computational coordinate system. If one applies a unit point force *exactly along the source–receiver line* (say $+y$ which corresponds to radial or North for `SALVUS`), then:

SH motion is not excited.

Mathematically this follows from cylindrical symmetry: if the force is colinear with the receiver azimuth, the radiation pattern contains only P–SV energy and the SH system is not driven. Consequently, a SALVUS simulation with a force purely aligned with the $+y$ direction produces:

$$u_y(t) \neq 0, \qquad u_z(t) \neq 0, \qquad u_x(t) \approx 0.$$

This matches theoretical expectations and is consistent with the transverse component of QSEIS being identically zero when the horizontal force has no transverse projection.

To reproduce the `QSEIS` *transverse* Green's function using `SALVUS`, a second simulation must be run with the point force applied in the direction *perpendicular* to the receiver line, e.g. along $+x$. This excites solely SH motion and yields:

$$u_x^{(SH)}(t) \neq 0, \qquad u_y^{(SH)}(t) \approx 0, \qquad u_z^{(SH)}(t) = 0,$$

up to numerical noise. This component corresponds directly to the transverse Green's function $G_t^{(h)}$ output by QSEIS.

3.3 Why a force along the receiver line cannot generate SH motion

To emphasize the physical origin of this behavior, consider a point force applied along the azimuthal direction $\theta = 0$ toward the first receiver. In cylindrical coordinates (r, θ, z), the displacement field from such a force is axisymmetric with respect to that direction. The SH system corresponds to motion in the θ direction and satisfies a decoupled wave equation of the form:

$$\frac{\partial^2 u_\theta}{\partial t^2} = \beta^2 \nabla^2 u_\theta.$$

A radial or vertical force has no θ–component and therefore cannot act as a source term in the SH equation. Consequently, the SH field remains zero for all time unless an explicit transverse horizontal force is applied. `QSEIS` avoids this geometrical reasoning because it automatically decomposes a generic "horizontal" instruction into radial and transverse parts. `SALVUS` requires the user to specify these two directions separately.

3.4 Mapping QSEIS and SALVUS Green's functions

For later waveform synthesis, the correct correspondence is:

QSEIS output	SALVUS simulation
$G_z^{(v)}, G_r^{(v)}$	force applied vertically ($+z$)
$G_r^{(h)}, G_r^{(h)}$	force applied horizontally along receiver line ($+y$)
$G_t^{(h)}$	force applied horizontally perpendicular to receiver line ($+x$)

Thus two SALVUS runs are required to reconstruct the full QSEIS horizontal Green's function set: one for the in-line force, and one for the transverse horizontal force. Once these two runs are obtained, their components can be rotated into any coordinate system in exactly the same way that QSEIS Green's functions are handled.

4 Matching QSEIS and SALVUS Seismograms

In this section we describe the practical procedure used to bring the QSEIS and SALVUS Green's functions to the same effective source wavelet, so that the resulting seismograms can be compared trace by trace. The main steps are: (i) extraction of the relevant Green's functions, (ii) characterization and resampling of the source wavelets, (iii) frequency–domain deconvolution of the QSEIS wavelet and reconvolution with the SALVUS wavelet, (iv) bandpass filtering and trace normalization, and (v) time alignment.

4.1 Extraction of Green's functions

For a given velocity model and receiver geometry, QSEIS is first run to produce Green's functions for the desired source type and component. In the example shown here we focus on the transverse component generated by a horizontal force, i.e. the file `fh-2.tt` (although the same steps hold true for all other force types and the respective Green's function components), and extract the corresponding seismograms

$$u_Q(t, x_i)$$

for receiver offsets $x_i \in [10, 5000]\,\mathrm{m}$, all sampled at $\Delta t = 1/50\,\mathrm{s}$ (50 Hz).

Similarly, SALVUS is run with a horizontal force oriented perpendicular to the receiver line, and the corresponding transverse displacement component is extracted from the SALVUS output, yielding seismograms

$$u_S(t, x_i)$$

at the same receiver offsets. The SALVUS solver internally uses a high–sample-rate source time function (here sampled at 1000 Hz), but the output seismograms are written at 50 Hz, matching the QSEIS sampling interval.

4.2 Source wavelets for QSEIS and SALVUS

QSEIS uses a built–in causal source wavelet of the form

$$w_Q(t) = \begin{cases} \dfrac{2}{\tau}\,\sin^2\!\left(\dfrac{\pi t}{\tau}\right), & 0 < t < \tau, \\ 0, & \text{otherwise}, \end{cases} \tag{2}$$

where τ is the wavelet duration. In our configuration we use $\tau = 4\Delta t$, so that $w_Q(t)$ is represented by four non-zero samples at the beginning of the `QSEIS` time series. This wavelet is strongly causal and has a non-zero phase spectrum.

`SALVUS`, by contrast, uses a user–supplied source time function $w_S(t)$, typically a smooth, approximately zero–phase wavelet with a broad and nearly flat amplitude spectrum over the frequency band of interest. In our case, the `SALVUS` source wavelet is provided as a vector sampled at 1000 Hz; it is downsampled to 50 Hz in two stages (by factors 5 and 4), and then zero–padded to the common FFT length $N_{\mathrm{FFT}} = 2048$:

$$w_S[n], \quad n = 0, \ldots, N_{\mathrm{FFT}} - 1.$$

The `QSEIS` wavelet $w_Q(t)$ is likewise sampled at 50 Hz using Eq. (2) for $t = 0, \Delta t, 2\Delta t, 3\Delta t$, and zero elsewhere, and then zero–padded to the same FFT length to obtain $w_Q[n]$.

4.3 Frequency–domain wavelet deconvolution

Let $u_Q[n, x_i]$ denote the discrete QSEIS seismogram at offset x_i, and let $W_Q[k]$ and $W_S[k]$ denote the discrete Fourier transforms of $w_Q[n]$ and $w_S[n]$:

$$W_Q[k] = \mathcal{F}\{w_Q[n]\}, \qquad W_S[k] = \mathcal{F}\{w_S[n]\}, \quad k = 0, \ldots, N_{\mathrm{FFT}} - 1.$$

In the frequency domain, the `QSEIS` seismogram can be written schematically as

$$U_Q[k, x_i] \approx G[k, x_i]\, W_Q[k],$$

where $G[k, x_i]$ is the underlying (discrete) Green's function. To replace the `QSEIS` wavelet w_Q by the `SALVUS` wavelet w_S, we perform a wavelet deconvolution and reconvolution:

$$\tilde{U}_Q[k, x_i] = U_Q[k, x_i]\, \frac{W_S[k]}{W_Q^{\mathrm{reg}}[k]}, \tag{3}$$

where $W_Q^{\mathrm{reg}}[k]$ is a regularized (waterlevel) version of $W_Q[k]$, described below. The time–domain matched seismogram is then obtained by inverse FFT:

$$\tilde{u}_Q[n, x_i] = \mathcal{F}^{-1}\{\tilde{U}_Q[k, x_i]\}.$$

Waterlevel regularization

Direct division by $W_Q[k]$ can be unstable at frequencies where $|W_Q[k]|$ is small. To stabilize the deconvolution, we replace the amplitude of $W_Q[k]$ above a chosen cutoff frequency f_{cut} by a constant "waterlevel" while preserving its phase:

$$W_Q[k] = |W_Q[k]| e^{i\phi_Q[k]},$$

$$W_Q^{\mathrm{reg}}[k] = \begin{cases} W_Q[k], & f_k < f_{\mathrm{cut}}, \\ |W_Q(f_{\mathrm{cut}})|\, e^{i\phi_Q[k]}, & f_k \geq f_{\mathrm{cut}}, \end{cases}$$

where f_k denotes the frequency corresponding to index k. In our implementation we use $f_{\mathrm{cut}} = 10$ Hz, and the magnitude $|W_Q(f_{\mathrm{cut}})|$ is used as the waterlevel for all higher frequencies. Hermitian symmetry is explicitly enforced on $W_Q^{\mathrm{reg}}[k]$ so that $\tilde{u}_Q[n, x_i]$ remains real–valued.

Note that the target comparison band is 2 Hz to 8 Hz; the choice of $f_{\mathrm{cut}} = 10$ Hz therefore does not influence the waveforms in the analysis band, and only serves to stabilize the deconvolution at higher frequencies, which are subsequently removed by bandpass filtering.

For each receiver, Eq. (3) is applied to the `QSEIS` seismogram $u_Q[n, x_i]$, followed by an inverse FFT, yielding a new set of time–domain traces $\tilde{u}_Q[n, x_i]$ that now carry the `SALVUS` source wavelet.

4.4 Bandpass filtering and normalization

Both the SALVUS seismograms $u_S[n, x_i]$ and the `QSEIS`–derived matched seismograms $\tilde{u}_Q[n, x_i]$ are then filtered using the same zero–phase bandpass filter in the 2 Hz to 8 Hz frequency range:

$$u_S^{(2\text{–}8)}[n, x_i], \quad \tilde{u}_Q^{(2\text{–}8)}[n, x_i],$$

implemented by forward–backward application of the filter coefficients (`filtfilt` in MATLAB). This step suppresses any high–frequency artifacts introduced by the deconvolution and ensures that both data sets are strictly comparable in the analysis band.

For visualization, each trace is normalized by its maximum absolute amplitude:

$$\hat{u}_S[n, x_i] = \frac{u_S^{(2\text{–}8)}[n, x_i]}{\max_n |u_S^{(2\text{–}8)}[n, x_i]|}, \qquad \hat{\tilde{u}}_Q[n, x_i] = \frac{\tilde{u}_Q^{(2\text{–}8)}[n, x_i]}{\max_n |\tilde{u}_Q^{(2\text{–}8)}[n, x_i]|}.$$

A global sign flip is applied to the `QSEIS` traces where necessary to account for differences in the sign conventions between the two codes. This is sign flip must tbe applied only for the vertical component. (QSEIS) treats the downward vertical as positive, while `SALVUS` treats upward vertical as positive. No sign flips need to be applied for the horizontal components.

4.5 Time alignment

The `SALVUS` source wavelet is zero–phase and symmetric about $t = 0$, with significant support for both positive and negative times (here roughly ± 1 s). In contrast, the `QSEIS` wavelet (2) is strictly causal and occupies only the earliest part of the time axis. After the deconvolution–reconvolution step, the effective onset of the QSEIS traces is therefore shifted forward by half the temporal support of the `SALVUS` wavelet.

`SALVUS` seismograms are written on a time axis that includes negative times, reflecting the acausal portion of the symmetric source wavelet. These negative-time samples do not correspond to physically meaningful arrivals; rather, they represent the left-hand side of the zero–phase wavelet and simply introduce a uniform time delay if retained. For this reason, and because the `SALVUS` wavelet is exactly symmetric about $t = 0$, the physically relevant seismograms must be taken only for $t > 0$, after truncating the acausal part. Once this is done, the `SALVUS` time axis becomes consistent with the `QSEIS` convention, and the two data sets can be compared directly.

In practice, the downsampled `SALVUS` wavelet has length n_W samples at 50 Hz. To correct for the symmetric time support, we discard the first $(n_W + 1)/2$ samples of the matched `QSEIS` traces $\tilde{u}_Q^{(2\text{–}8)}[n, x_i]$, and adjust the corresponding time vector so that $t = 0$ aligns with the `SALVUS` seismograms (after truncating any negative times from the `SALVUS` output). After this shift, the `QSEIS`–based and `SALVUS` seismograms must agree in arrival times across all offsets, and any remaining differences are due to numerical dispersion or minor implementation details rather than source-time mismatches.

5 Comparison of Synthetic Green's Functions: `QSEIS` vs. `SALVUS`

To assess the consistency between the reflectivity–based solver `QSEIS` and the spectral-element solver `SALVUS`, we compare Green's functions computed for an identical elastic model and source–receiver geometry. We begin with the simplest configuration—a homogeneous half-space—where theoretical expectations are well understood and numerical artifacts are minimal.

5.1 Homogeneous Half–Space Model

Both solvers employ the same uniform elastic medium, defined in Table 1. Attenuation is included in both simulations using identical quality factors, although in this low-frequency band (2–8 Hz) attenuation has negligible influence on the waveforms.

Table 1: Homogeneous half–space parameters used for the comparison.

Depth (km)	v_p (km/s)	v_s (km/s)	ρ (g/cm^3)	Q_p	Q_s
0.000 – ∞	4.000	2.000	2.465	900	450

Receivers are placed along the free surface from $x = 10$ m to $x = 5000$ m, with a total of 480 receiver positions. In all comparisons, `QSEIS` traces are deconvolved and reconvolved with the `SALVUS` wavelet as described in Section 4, filtered between 2–8 Hz, and normalized by per–trace maximum amplitude.

5.1.1 Case 1: Vertical Force – Vertical Component $G_z^{(v)}$

A vertical point force at the free surface excites only Rayleigh waves and P–SV body waves. Thus the comparison of the vertical Green's function $G_z^{(v)}$ represents a clean low–mode Rayleigh problem.

Figure 2 shows the gathers obtained from `QSEIS` and `SALVUS`. Every fifth receiver trace is displayed for clarity (corresponding to an approximate spacing of 160 m). The waveforms exhibit excellent agreement: the direct P and S arrivals match in phase and amplitude, and the fundamental-mode Rayleigh wave shows virtually identical group and phase velocities.

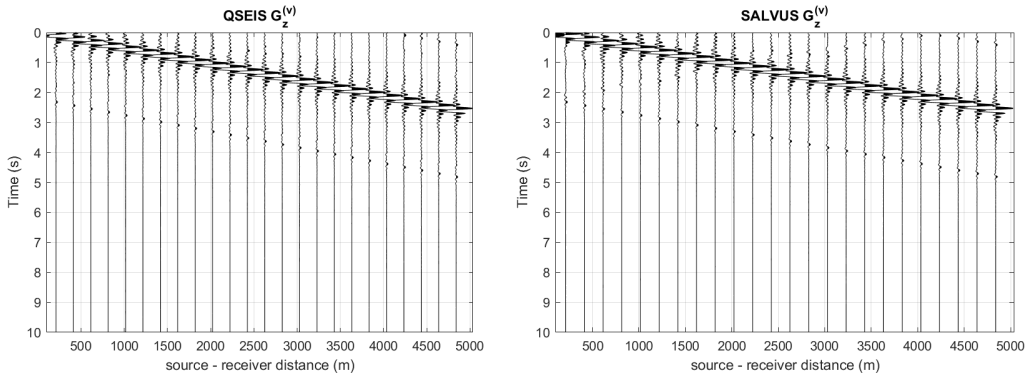

Figure 2: Comparison of vertical $G_z^{(v)}$ gathers for a horizontal point force in a homogeneous half–space corresponding to both the source and receivers laid out on the free surface. Left: `QSEIS`; right: `SALVUS`. Traces are plotted every 5 receivers for clarity.

To demonstrate the waveform fidelity more directly, Figure 3 compares individual traces at two representative offsets: (1) $x = 372.17$ m, where both near–field and early Rayleigh motion are present; and (2) $x = 5000$ m, where the far–field Rayleigh wave dominates. The agreement is nearly perfect in both cases, confirming that the wavelet treatment, time alignment, and amplitude normalization procedures produce physically consistent signals.

5.1.2 Case 2: Horizontal Force – Radial Component $G_r^{(h)}$

For a horizontal point force applied along the source–receiver line, only P–SV motion is physically generated. (`QSEIS`'s default horizontal-force operator produces both radial and transverse outputs;

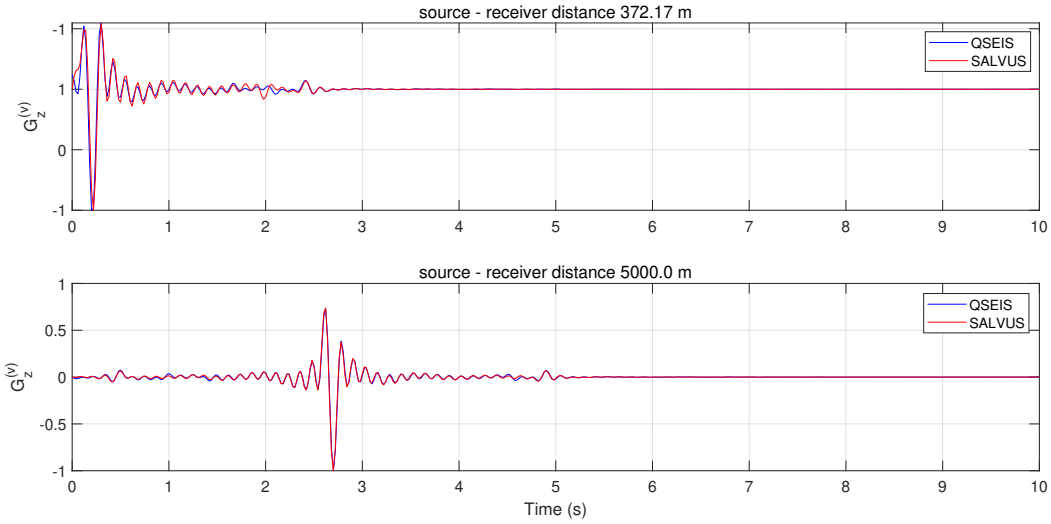

Figure 3: Trace-by-trace comparison of the vertical Green's function $G_r^{(h)}$ due to a vertical point force in a homogeneous half-space for offsets of 372.17 m (top) and 5000 m (bottom). Blue: `QSEIS`; red: `SALVUS`. Both the sources and the receivers are spread on the free surface.

however, as discussed in Section 3, its transverse component corresponds to a mathematically separate orthogonal horizontal force and not a single physical load.)

Using a purely radial force in `SALVUS`, we compare the resulting radial Green's function $G_r^{(h)}$. The comparison again shows excellent agreement between the two solvers, with matched arrival times, radiation patterns, and Rayleigh-wave dispersion characteristics. Figures analogous to Figs. 2–3 demonstrate the same level of correspondence as in the vertical-force case.

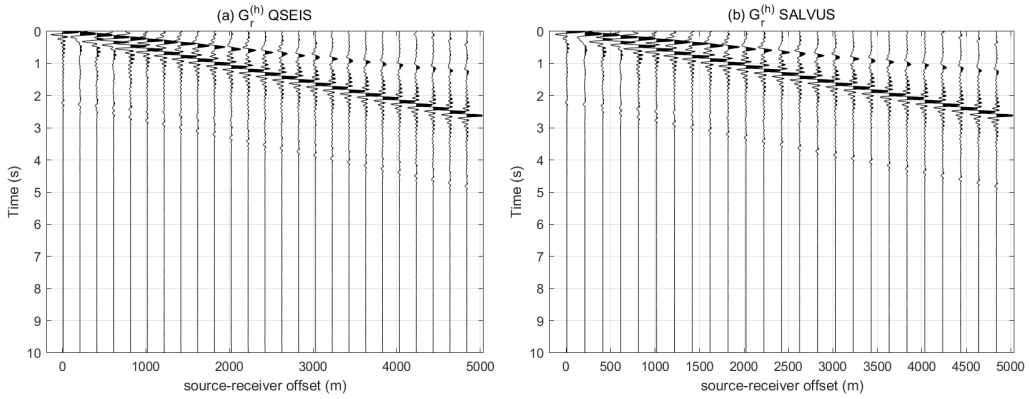

Figure 4: Comparison of radial $G_r^{(h)}$ gathers for a horizontal point force in a homogeneous half–space corresponding to both the source and receivers laid out on the free surface. Left: `QSEIS`; right: `SALVUS`. Traces are plotted every 5 receivers for clarity.

These results confirm that, after correcting for wavelet, timing, and coordinate conventions, `QSEIS` and `SALVUS` produce indistinguishable Green's functions for a homogeneous half–space. This forms the baseline for the subsequent layered-medium comparison.

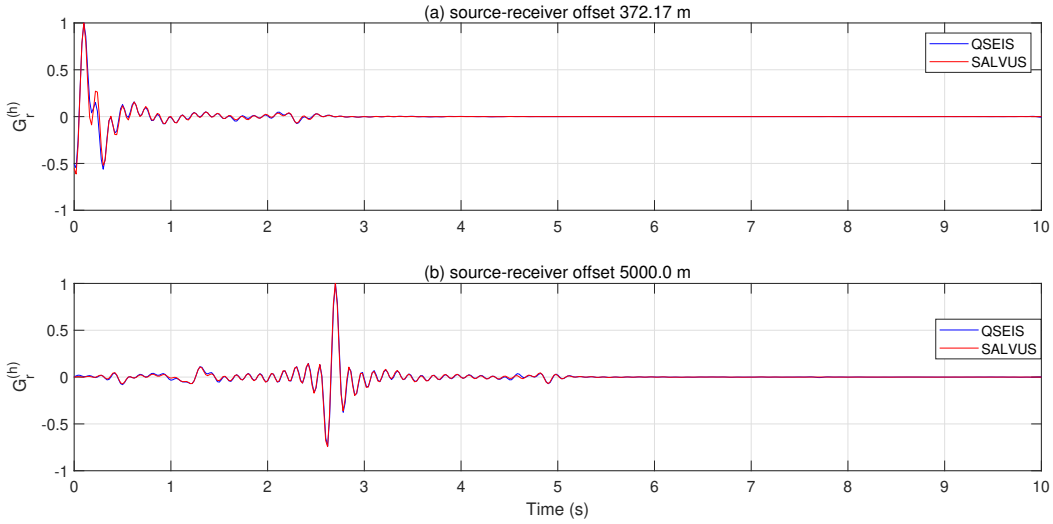

Figure 5: Trace-by-trace comparison of the radial Green's function $G_r^{(h)}$ due to a horizontal force in a homogeneous half-space for offsets of 372.17 m (top) and 5000 m (bottom). Blue: `QSEIS`; red: `SALVUS`. Both the sources and the receivers are spread on the free surface.

5.2 Layered Half space with small intrinsic attenuation

In this section, we present a comparison of synthetic seismograms computed for a layered half–space model. As in the homogeneous case, we compare results obtained with `QSEIS` and `SALVUS` for different source types and Green's function components. The elastic properties of the layered model are summarized in Table 2. This model is intended to represent a layered half–space with little intrinsic attenuation, hence we assign uniform quality factors of $Q_P = 10000$ and $Q_S = 5000$ in all layers. These large Q values allow us to focus on waveform consistency between the two solvers rather than on amplitude decay due to attenuation (which is a separate test and presented later in this note).

As in the homogeneous case, we consider two representative configurations: (1) a vertical point force with analysis of the vertical Green's function component, and (2) a horizontal point force with analysis of the transverse Green's function component.

Table 2: Layered half–space parameters used for the comparison.

Depth (km)	v_p (km/s)	v_s (km/s)	ρ (g/cm^3)	Q_p	Q_s
0.030	1.000	0.500	1.743	10000	5000
0.120	3.000	1.500	2.294	10000	5000
0.300	4.500	2.500	2.539	10000	5000
1.000	5.000	3.000	2.606	10000	5000
5.000	5.800	3.360	2.720	10000	5000
∞	6.000	3.500	2.800	10000	5000

5.2.1 Case 1: Vertical force – Vertical component $G_z^{(v)}$

In this configuration, a vertical point force is applied at the free surface, and the resulting displacement field is recorded at 480 surface receivers uniformly distributed between 10 m and 5000 m

offset. Figures 6(a) and (b) show the resulting Green's function gathers obtained with `QSEIS` and `SALVUS`, respectively. These gathers are characterized by multiple dispersive wave trains. In particular, the slowest arrivals reach the farthest receivers at travel times between approximately 25 and 30 s, corresponding to extremely low apparent group velocities on the order of 150–200 m/s. To interpret these arrivals, we compute the theoretical Rayleigh-wave dispersion curves for the layered model in Table 2.

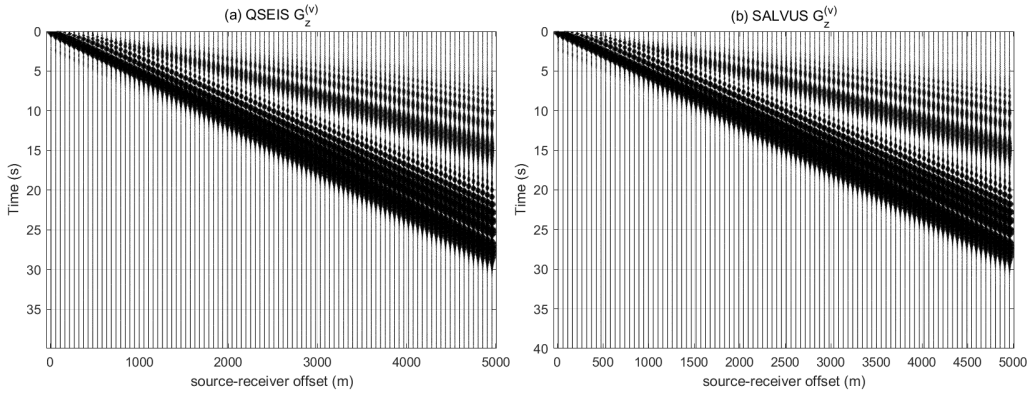

Figure 6: Comparison of $G_z^{(v)}$ gathers for a vertical point force in a layered half–space corresponding to both the source and receivers laid out on the free surface. Left: `QSEIS`; right: `SALVUS`. Traces are plotted every 5 receivers for clarity. Slow propagating Rayleigh wave energy is visible in both the gathers.

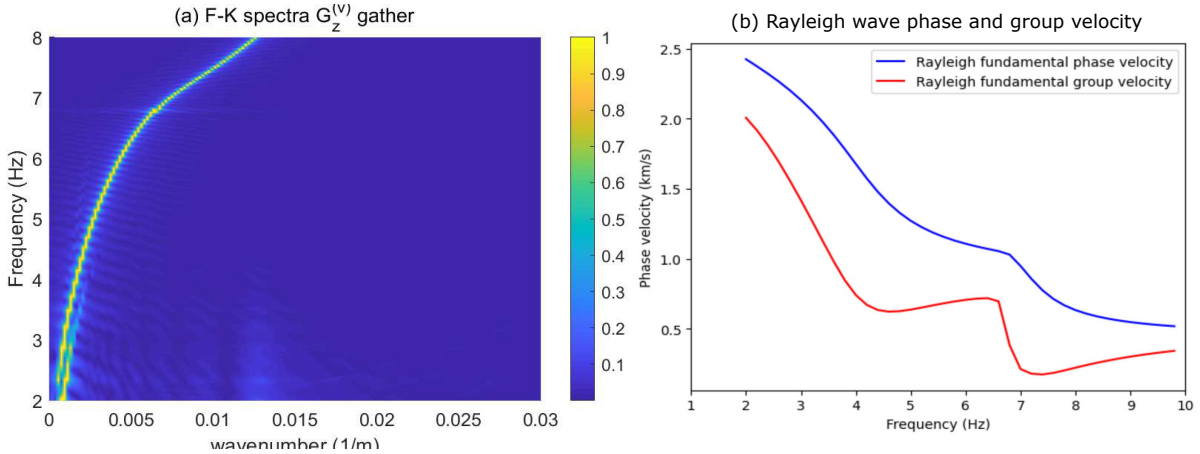

Figure 7: (a) Frequency–wavenumber (F–K) spectrum of the shot gather shown in Figure 6, highlighting the fundamental Rayleigh mode within the 2–8 Hz band. (b) Theoretical phase (blue) and group (red) velocity curves for the layered model in Table 2. The very slow group velocities in the 6–8 Hz band explain the late-arriving wave trains observed in the shot gathers.

Figure 7(b) shows the fundamental-mode Rayleigh phase and group velocities. The frequency band between 6 and 8 Hz is characterized by very slow group velocities, which directly explains the late-arriving, high-energy wave trains observed in the shot gathers. In contrast, the corresponding phase velocities remain significantly higher, reaching values of approximately 650 m/s at 8 Hz. This distinction between slow group velocity and faster phase velocity is further confirmed by the

frequency–wavenumber (F–K) spectrum shown in Figure 7(a), where the fundamental Rayleigh mode is clearly visible within the 2–8 Hz analysis band.

Finally, Figures 8(a) and (b) show a trace-by-trace comparison of the vertical Green's function $G_z^{(v)}$ at offsets of 103.75 m and 5000 m, respectively. The waveforms produced by `QSEIS` and `SALVUS` are virtually indistinguishable, exhibiting excellent agreement in both phase and amplitude across the entire time window.

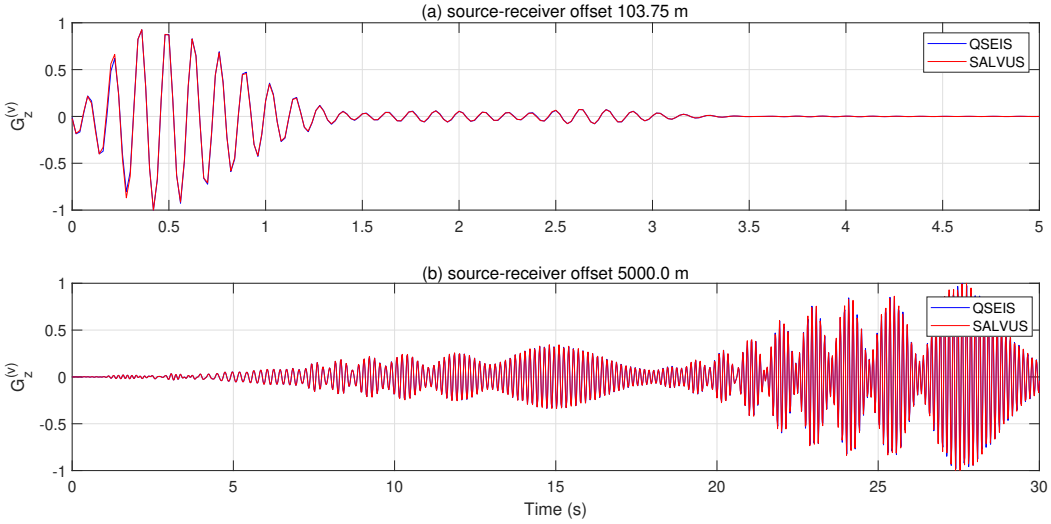

Figure 8: Trace-by-trace comparison of the vertical component of the Green's function $G_z^{(v)}$ in a layered half-space for source-receiver offsets of (a) 103.75 m and (b) 5000 m. Blue: `QSEIS`; red: `SALVUS`. Both the source and the receivers are spread on the free surface.

5.2.2 Case 2: Horizontal force – transverse component

The test case of a horizontal force acting on the surface, the transverse component of the ground motion shows the SH wave-type propagation. Similar to the previous case we have 480 receivers equally spaced between 10 and 5000 m on the surface. Love waves being the most dominating SH wave propagation type on the surface, we expect the recordings to be dominated by Love waves. Figures 9(a) and (b) show the Green's function gathers generated using `QSEIS` and `SALVUS`, respectively. Unlike the previous scenario presented, the slowest wave-train observed correspond to the Love waves which for this particular subsurface model parameters exhibit faster group velocities than the Rayleigh waves and hence arrive at the farthest stations much earlier (for the previous case it was between 25 – 30 s). For trace by trace comparison we also present the individual seismograms generated by `QSEIS` and `SALVUS` corresponding to source receiver offsets of 103.75 m and 5000.0 m (Figures 10(a) and (b)). At both offsets, the `QSEIS` and `SALVUS` seismograms are indistinguishable and match both in phase and amplitude.

5.3 Layered Half-space with realistic intrinsic attenuation

The final comparison of synthetic seismograms between `QSEIS` and `SALVUS` is presented for the case of layered half-space with realistic intrinsic attenuation. Table 3 shows the subsurface parameters for the layered half-space model. We keep the V_p, V_s, and ρ the same as the previous test, however,

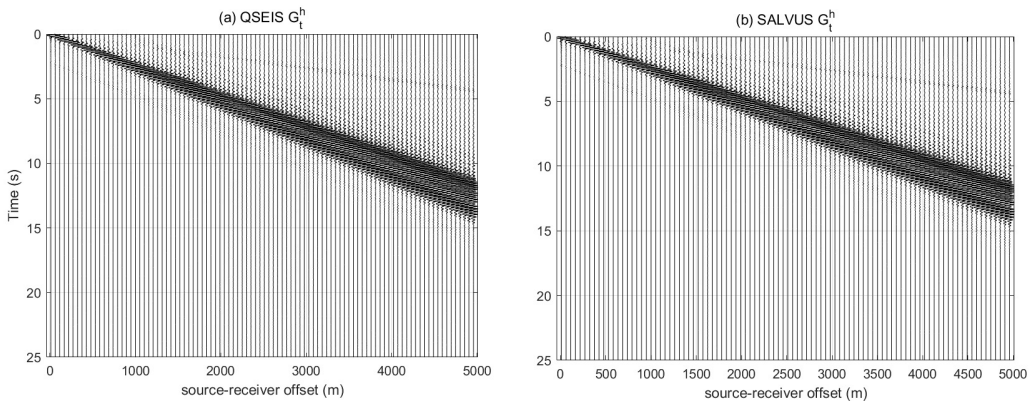

Figure 9: Comparison of $G_t^{(h)}$ gathers for a horizontal point force in a layered half–space corresponding to both the source and receivers laid out on the free surface. Left: `QSEIS`; right: `SALVUS`. Traces are plotted every 5 receivers for clarity. Strong Love wave energy is visible in both the gathers.

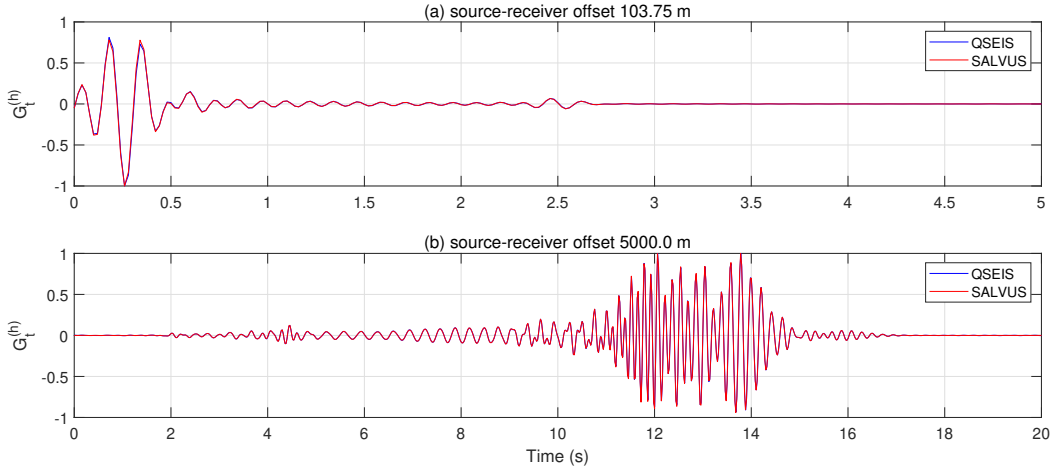

Figure 10: Trace-by-trace comparison of the transverse component of the Green's function $G_t^{(h)}$ in a layered half-space for source-receiver offsets of (a) 103.75 m and (b) 5000 m. Blue: `QSEIS`; red: `SALVUS`. Both the source and the receivers are spread on the free surface.

the Q_p and Q_s values are modified to represent realistic intrinsic attenuation mimicking both shallower and deeper sediments. The soft soil on the top most layer is assigned a small value of $Q_s = 50$, and Q_p is set at twice the Q_s value. This is typical of unconsolidated sediments with high porosity and shale content. The Q-values are increased gradually per layer, implying weaker attenuation as we go deeper.

6 Discussion

The observed time shift is fully explained by the difference in source-time-function definition. QSEIS uses a short, causal pulse whose center of energy is delayed by $\tau/2$ relative to a zero-phase pulse. SALVUS, using a symmetric wavelet, produces zero-lag output.

Because this difference is source-related rather than physical, it appears uniformly in all com-

Table 3: Layered half–space parameters with realistic p and S-wave intrinsic attenuation.

Depth (km)	v_p (km/s)	v_s (km/s)	ρ (g/cm^3)	Q_p	Q_s
0.030	1.000	0.500	1.743	100	50
0.120	3.000	1.500	2.294	250	125
0.300	4.500	2.500	2.539	400	200
1.000	5.000	3.000	2.606	600	300
5.000	5.800	3.360	2.720	900	450
∞	6.000	3.500	2.800	1200	600

ponents, offsets, and phases. Removing it yields nearly indistinguishable waveforms from both solvers.

Importantly, the consistency of SALVUS and QSEIS after delay correction confirms that:

- both solvers correctly propagate elastic waves in a homogeneous medium,
- numerical dispersion and attenuation are negligible in this test,
- solver differences do not accumulate with distance,
- any residual difference comes from details of wavelet implementation, not physics.

7 Appendix: Derivation of the QSEIS Time Shift

The default QSEIS wavelet

$$w(t) = \frac{2}{\tau}\,\sin^2\!\left(\frac{\pi t}{\tau}\right), \qquad 0 < t < \tau, \tag{4}$$

is defined only on the interval $[0, \tau]$. Using the identity $\sin^2 x = \frac{1}{2}(1 - \cos 2x)$,

$$w(t) = \frac{1}{\tau}\left(1 - \cos\frac{2\pi t}{\tau}\right). \tag{5}$$

Let $u = t - \frac{\tau}{2}$, so that $t = u + \tau/2$. Then

$$\cos\frac{2\pi t}{\tau} = \cos\!\left(\frac{2\pi}{\tau}(u + \tfrac{\tau}{2})\right) = \cos\!\left(\frac{2\pi u}{\tau} + \pi\right) = -\cos\frac{2\pi u}{\tau}. \tag{6}$$

Substituting,

$$w(t) = w(u + \tfrac{\tau}{2}) = \frac{1}{\tau}\left(1 + \cos\frac{2\pi u}{\tau}\right), \qquad -\tfrac{\tau}{2} < u < \tfrac{\tau}{2}. \tag{7}$$

This function is even in u, hence its Fourier transform has (approximately) zero phase. Therefore, the original QSEIS wavelet $w(t)$ is equivalent to a *zero-phase* wavelet $\widetilde{w}(u)$ shifted in time by $\tau/2$:

$$w(t) = \widetilde{w}(t - \tfrac{\tau}{2}). \tag{8}$$

In the frequency domain, this becomes

$$W(\omega) = e^{-i\omega\tau/2}\,\widetilde{W}(\omega), \tag{9}$$

so the QSEIS source spectrum contains a pure time delay of $\tau/2$.

For the default choice $\tau = n_{\mathrm{sam}}\,\Delta t = 0.08\,\mathrm{s}$, the delay is

$$\Delta t = \frac{\tau}{2} = 0.04\,\mathrm{s}, \tag{10}$$

corresponding to two samples at 50 Hz. This delay propagates into all synthetic seismograms generated by QSEIS when the default source-time function is used.